Effective mass enhancement and ultrafast electron dynamics of Au(111) surface state coupled to a quantum well

A. Varykhalov,[1] F. Freyse,[1,2] I. Aguilera,[3] M. Battiato,[4] M. Krivenkov,[1,2] D. Marchenko,[1] G. Bihlmayer,[3] S. Blügel,[3] O. Rader,[1] and J. Sánchez-Barriga[1,*]

[1]*Helmholtz-Zentrum Berlin für Materialien und Energie, BESSY II, Albert-Einstein-Str. 15, 12489 Berlin, Germany*
[2]*Institut für Physik und Astronomie, Universität Potsdam, Karl-Liebknecht-Str. 24/25, 14476 Potsdam, Germany*
[3]*Peter Grünberg Institute and Institute for Advanced Simulation, Forschungszentrum Jülich and JARA, D-52425 Jülich, Germany*
[4]*Nanyang Technological University, Nanyang Link 21, 637371, Singapore*

We show that while the equilibrium band dispersion of the Shockley-type surface state of two-dimensional Au(111) quantum films grown on W(110) does not deviate from the expected free-electron-like behavior, its nonequilibrium energy-momentum dispersion probed by time- and angle-resolved photoemission exhibits a remarkable kink above the Fermi level due to a significant enhancement of the effective mass. The kink is pronounced for certain thicknesses of the Au quantum well and vanishes in the very thin limit. We identify the kink as induced by the coupling between Au(111) surface state and emergent quantum-well states which probe directly the buried gold−tungsten interface. The signatures of the coupling are further revealed by our time-resolved measurements which show that surface state and quantum-well states thermalize together behaving as dynamically-locked electron populations. In particular, relaxation of hot carriers following laser excitation is similar for both surface state and quantum-well states and much slower than expected for a bulk metallic system. The influence of quantum confinement on the interplay between elementary scattering processes of the electrons at the surface and ultrafast carrier transport in the direction perpendicular to the surface is shown to be the reason for the slow electron dynamics.

I. INTRODUCTION

The Au(111) surface state is one of the most prominent examples of Shockley-type surface states [1–4]. It is supposed to have an ideal parabolic band dispersion which is well described in terms of the free-electron-like approximation, and a spin-orbit splitting on a scale of $\sim$100 meV which is caused by the Rashba-Bychkov effect [5, 6] due to the high atomic number of Au [7, 8]. Recently, an alternative description of the Au(111) surface state in the framework of topological theory of solids was proposed [9]. Based on the connectivity of the surface state to the bulk bands far above the Fermi level and relying on the parity analysis of the calculated band structure [9], the Au surface state was identified as topologically nontrivial owing to the predicted Z_2-type invariants of Au [9]. Although the model appears elegant it can be applied only conditionally, because without an artificial increase of spin-orbit coupling strength [9] bulk Au(111) does not exhibit a continuous band gap along the time-reversal-symmetric direction of its surface Brillouin zone [10]. This fact, in turn, precludes a topological description from the dispersion of the Au(111) surface state. Especially for metals, the situation is nevertheless controversial as in the most general case the surface-state deviation from a parabolic band dispersion and its connectivity to the bulk bands do not necessarily imply topological protection [11]. An important example is the Rashba-split surface state of Ir(111), where the connectivity and parity of the bands resemble those of a topological system [12, 13].

In this work, we experimentally follow the dispersion of the Au surface state beyond the Fermi level E_{F}, finding a remarkable deviation of the Au surface state (SS) band dispersion from the expected free-electron-like behavior. We show that in a purely two-dimensional Au(111) film forming a quantum cavity grown on W(110), the SS can couple to quantum-well states (QWSs) residing inside the cavity and, as a result of the interaction of QWSs with the substrate, the SS acquires a significant renormalization of its effective mass. Our main finding is a kink structure in the energy-momentum dispersion E(**k**) of the SS which is observed as a deviation from a naturally parabolic band which is demonstrated to be not related to topological properties but – even for thick quantum films – to the substrate. We further show that such coupling requires proximity of the SS to QWSs in energy-momentum space and hence the kink vanishes at small thickness (i.e., small width of the quantum well). As the kink resides within the unoccupied band structure, we use time- and angle-resolved photoemission (tr-ARPES) to access the band dispersion above E_{F}. The signatures of the coupling are also evidenced by our measurements of the ultrafast electron dynamics, which reveal that the renormalized SS and QWSs behave as dynamically-locked electron populations exhibiting universal relaxation times significantly slower than expected for a bulk metallic system.

II. METHODS

We performed tr-ARPES experiments using linearly-polarized 1.5 eV pump and 6 eV probe femtosecond (fs)-laser pulses. The pulses were generated with a homemade Ti: Sapphire fs oscillator coupled to an ultrafast amplifier laser system (RegA, Coherent) operated at 150 kHz repetition rate. The time delay Δt between pump and probe pulses was varied using an optical delay stage. The time resolution

of the experiment was ∼200 fs, and the pump fluence ∼100 μJ/cm^2. Additional synchrotron-based ARPES measurements were carried out using linearly-polarized undulator radiation at the U125-2-PGM beamline of BESSY-II in Berlin. Photoelectrons were detected with a Scienta R4000 analyzer at the RGBL-2 end station and the base pressure of the experimental setup was better than 1×10^{-10} mbar. The angular and energy resolutions of the photoemission experiments were 0.1° and 20 meV, respectively. Au(111) quantum films were grown by deposition of 1-16 nm of Au on W(110) as described elsewhere [14]. Density functional theory (DFT) calculations were carried out within the all-electron full-potential linearized augmented-plane-wave formalism as implemented in the FLEUR [15] code. We used the Perdew-Burke-Ernzerhof (PBE) functional, an angular momentum cutoff of $l_{\max} = 10$ in the atomic spheres and a plane-wave cutoff of 3.5 bohr^{-1}. Strain was simulated in all directions by rescaling the lattice constant. All calculations were performed for a freestanding 4 nm-thick Au slab. Scanning tunneling microscopy (STM) studies were conducted with an Omicron VT STM using a polycrystalline tungsten tip prepared as detailed elsewhere [16].

III. RESULTS AND DISCUSSION

A. Equilibrium band structure

Figure 1(a) shows the SS of a 7 nm-thick Au(111) quantum film grown on W(110) as seen by ARPES in equilibrium (no pump photons) along the $\overline{\Gamma}-\overline{\mathrm{K}}$ direction of the surface Brillouin zone (SBZ) [Fig. 1(d)]. The parabolic dispersion of the SS with the band bottom located at the $\overline{\Gamma}$ point of the SBZ and at ∼0.43 eV binding energy is clearly visible. The bands next to the SS correspond to QWSs [14, 17–22] occurring due to confinement of *sp* electrons in the potential well of the film. The Fermi surface map in Fig. 1(b) shows a characteristic onion-like arrangement of sharp QWSs around the circular contour of the SS confirming the excellent structural quality of the quantum cavity. The homogeneous thickness of the Au film is also revealed by our STM images [Figs. 1(e) and 1(f)]. In particular, the dark hexagonal spots are surface features of only 1–2 monolayer (ML) deep. In agreement with previous studies on Au quantum films [23], the Rashba-type spin-orbit splitting of the SS is not observed. We attribute this effect to an enhanced electron scattering at a network of surface distortions occurring due to strain, which is induced in the Au film by the low-symmetric W(110) substrate. These distortions, which might be responsible for lateral modulations of the electron wave function [24, 25], occur as arrays in domains with different orientations [Fig. 1(c)] and have a periodicity of ∼25-30Å as seen from the zoomed STM image shown in Fig. 1(f). The superstructure can be identified as a reshaped herringbone $(22\sqrt{3})$ reconstruction. Interestingly, we observe such dislocations more ordered than in earlier STM works [26]. Their well-defined periodicity is also confirmed by the perfectly-ordered superstructural constellations seen by low-energy electron diffraction (LEED) [Fig. 1(c)].

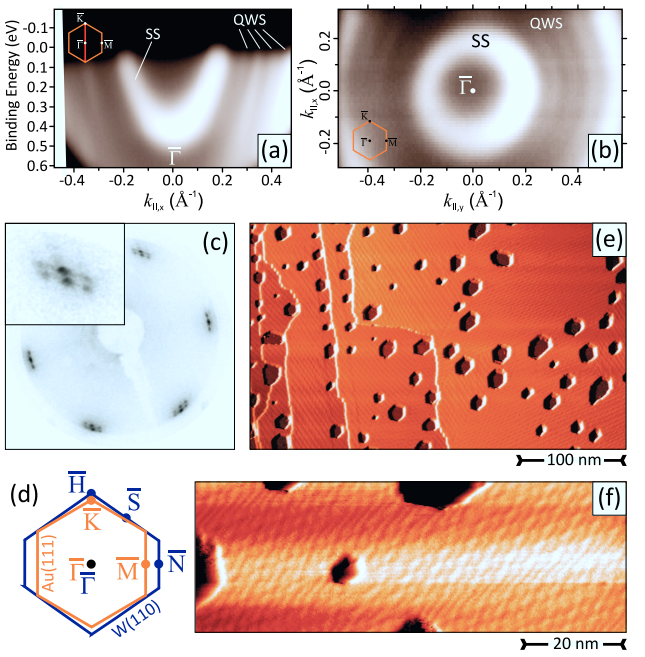

FIG. 1. Gold quantum films on W(110). (a) Au(111) surface state (SS) of a 7 nm-thick film measured in equilibrium by ARPES at 6 eV photon energy. The multiple sharp bands next to it are quantum-well states (QWSs) occurring due to perpendicular-to-the-surface confinement of *sp* electrons. (b) At the Fermi surface, both SS and QWSs form onion-like perfectly concentric contours. (c) Low-energy electron diffraction reveals sharp spots of Au(111) surrounded by a spatially anisotropic superstructure originating from a herringbone reconstruction $(22\sqrt{3})$ modified by the strain induced from the substrate. (d) Sketch of the surface Brillouin zone of Au(111) [orange] and W(110) [violet] in mutual correspondence. (e),(f) Scanning tunneling microscopy (STM) images. In (f), a zoom-in on the herringbone-derived reconstruction is shown.

B. Kink structure above E_F

Figure 2(a) shows the energy-momentum band dispersion of Au SS and QWSs measured by tr-ARPES at Δt=0 fs for different widths of the quantum well. The unoccupied part of the band structure is now transiently populated with excited electrons and can be accessed directly. While for a narrow potential well [1 nm film, left panel in Fig. 2(a)] a parabolic dispersion of the Au SS is seen, a deviation from this behavior can be identified with increasing quantum-well thickness.

In particular, at energies of ∼0.15 eV above E_F, the SS dispersion exhibits a kink structure and the electron group velocity decreases, evidencing a significant enhancement of the effective mass. The accurate extraction of the photoemission peaks along with parabolic fits of the band dispersion [Fig. 2(b)] reveals that due to the kink structure the effective mass of the SS increases by about a factor of 2 within the band itself, i.e. from ∼0.33−0.36 m_e [blue lines] to ∼0.63−0.53 m_e [red lines]. Here m_e denotes the free-electron mass. Interestingly, at 1 nm thickness [left panels in Figs. 2(a) and 2(b)], the effective mass of the whole SS band increases up to ∼ 0.51 m_e. We attribute this effect to the influence of strain, which in

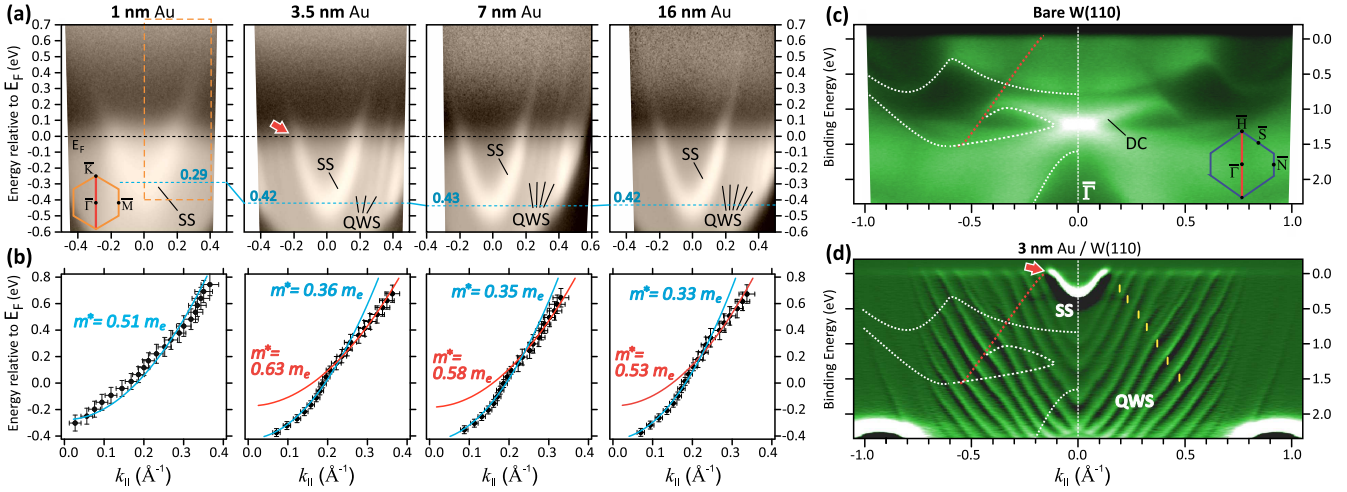

FIG. 2. (a) From left to right, tr-ARPES spectra of Au(111) quantum films of different thicknesses measured at Δt=0. The energy-momentum dispersions of surface state and quantum-well states are labelled as SS and QWS, respectively. (b) Band dispersions of Au SS extracted from (a). The kink structure in the SS dispersion corresponds to an enhancement of the effective mass from $\sim$0.36$-$0.33 m_e [blue lines] to $\sim$0.63$-$0.53 m_e [red lines]. (c,d) Band structures of (c) bare W(110) and (d) 3 nm-thick Au film on W(110) measured with synchrotron radiation at 62 eV photon energy. The linearly dispersing band edge of W (red dashed line) causes kinks in the QWS bands (yellow ticks). It is also responsible for the kink in the SS due to SS-QWS coupling (see text for details). White dashed lines mark the edges of the bulk W gap projected onto the (110) surface. The directions of the surface Brillouin zones of Au(111) and W(110) along which the band structures are sampled are indicated with red solid lines in the insets of (a) and (c), respectively.

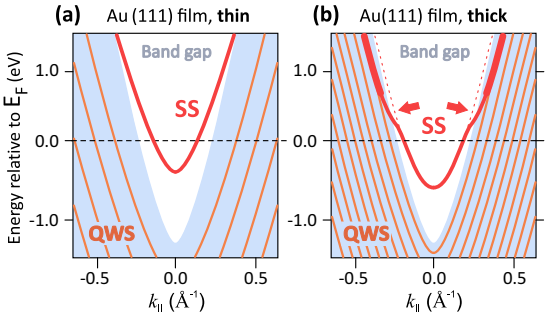

FIG. 3. Sketch illustrating the coupling between Au(111) surface state (SS) and quantum-well states (QWSs) in Au quantum films. (a) For extremely thin films the spectrum is discrete but SS (red line) and QWS bands (orange lines) have large separation in energy-momentum space, and the coupling is weak. (c) For thicker Au quantum films the number of QWS bands increases, reducing the separation and enhancing the coupling, thereby giving rise to a kink structure in the SS dispersion (red arrows). The vanishing spin-orbit splitting is based on the experimental findings (see text).

addition causes the energy shift of the SS dispersion [horizontal blue dashed lines in Fig. 2(a)] and the surface distortions responsible for the broadening of the SS peaks.

C. Relevance of QWSs for the kink structure

The overall behavior of the energy-momentum dispersion of the SS seen in Figs. 2(a) and 2(b) indicates that QWSs and their coupling to the SS are highly relevant for the appearance of the kink structure. Indeed, the width of the quantum cavity defined by the Au thickness determines the electron confinement and hence the discrete energy spectrum of QWSs. One can thus assume that at certain thickness, the QWS band residing closer to the border of surface-projected band gap of Au(111) approaches the SS band localized therein and couples to it causing the kink. This effect is qualitatively illustrated in Fig. 3, which shows a schematic representation of the electronic band structures of thin [Fig. 3(a)] and thick [Fig. 3(b)] Au(111) quantum films. In line with this assumption, it was earlier shown that the SS of Cu(111) can gain effective mass even due to coupling to non-confined states of the bulk [27], however no kink structure exists in the bulk limit [9, 27] and the mass enhancement is much stronger in the case of coupling to QWSs as shown in the present work.

D. Influence of strain on the SS and its topological character

To understand whether the kink structure is inherent to the quantized electronic structure of Au(111), we performed model DFT calculations for a 4 nm-thick Au slab as shown in Fig. 4. In the course of the simulation, we changed the binding energy of the SS via small variations of the lattice constant, simulating in this way the strain induced in the Au film by the W substrate. This allowed us to move the Au SS band close to the region above E_F near the border of the Au(111) surface band gap and, accordingly, closer to the QWS band with lowest binding energy. One can see that, while the energy spectrum of QWSs is less perturbed by such a change, the SS band dispersion reacts very sensitively [28].

Figure 4 shows four panels corresponding to different grades of strain induced in the Au slab: zero strain [Fig. 4(a)], expansive strain of +1% [Fig. 4b)], compressive strain of -5% [Fig. 4(c)] and extreme compressive strain of -10% [Fig. 4(d)].

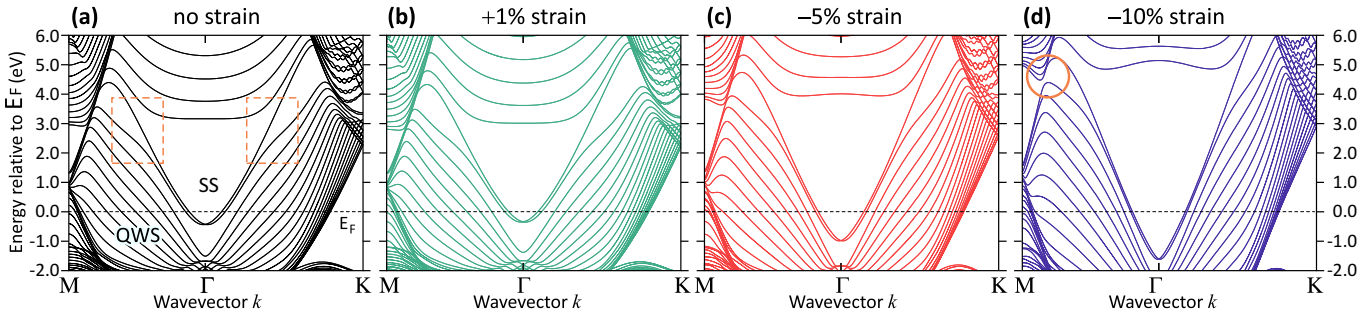

FIG. 4. Density-functional theory (DFT) calculations of the band structure of a 4 nm-thick Au slab subjected to different grades of strain. (a) No strain, (b) expansive strain of +1%, (c) compressive strain of -5%, (d) extreme compressive strain of -10%. Strain causes an energy shift of the surface state (SS) band dispersion, a change in its effective mass and a reduction of the spin splitting. The deviation from free-electron-like behavior in the SS dispersion becomes more pronounced close to the region where the SS connects to quantum-well state (QWS) bands [orange dashed rectangles in (a)]. For an extremely strained Au film in (d), the opening of an inverted band gap along the time-reversal-invariant direction $\overline{\Gamma} - \overline{\mathrm{M}}$ [orange circle] is shown by the connectivity of the bands.

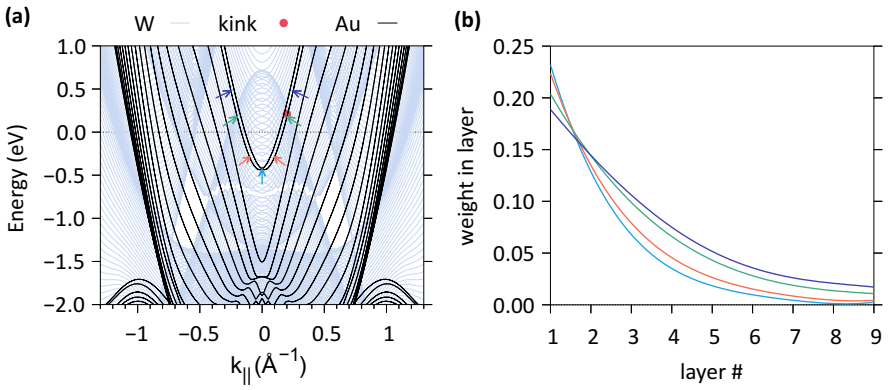

FIG. 5. (a) DFT calculation of bulk W projected on the surface Brillouin zone (gray) compared to the bands of a 4 nm Au slab as in Fig. 4(a) in the direction $\overline{\Gamma} - \overline{\mathrm{K}}$. (b) **k**-dependent decay of the SS wave function within the 4 nm slab. The red circle in (a) indicates the position of the experimentally observed kink. The colored arrows in (a) indicate the energy-momentum points at which the curves in panel (b) are obtained.

Strain not only causes an energy shift of the SS dispersion and a change of its effective mass, but also a reduction of the spin splitting. These findings, which are qualitatively in line with our experimental results of Fig. 2, are related to the fact that strain directly affects orbital hybridization [24, 25]. The effect also manifests at energies of ∼2–4 eV above E_{F} [region marked with orange dashed rectangles in Fig. 4(a)], where there is strong deviation of the free-electron-like character of the SS dispersion. In particular, one of the spin-subbands of the Rashba-split SS is more affected by the interaction with the QWS which is closest to it in energy-momentum space, pinpointing the importance of the coupling. Conversely, from the results in Fig. 4, one can also see that the SS kink at ∼0.15 eV above E_{F} is negligible. This result is surprising considering that the calculation captures qualitatively most of the relevant aspects of the experimental band dispersion of Fig. 2, namely (i) the energy shift of the SS, (ii) the change in its effective mass, (iii) the vanishing spin splitting, and (iv) the importance of the coupling between SS and QWS bands. Therefore, we conclude that the origin of the kink structure in Fig. 2 must be necessarily related to the quantized electronic structure of Au(111), but in a much more complex way, as we will discuss further below.

We also point out that the calculation in Fig. 4 shows no global band gap opening at high energy, as evidenced in the entire Brillouin zone by the fact that QWSs do not disperse in the direction perpendicular to the surface. This situation is also the case of an extremely strained (-10%) Au film [Fig. 4(d)], which exhibits a local band gap opening only in the region marked with an orange dashed circle in Fig. 4(d). On this basis, taking into account that the $\overline{\Gamma} - \overline{\mathrm{M}}$ direction of the Au(111) SBZ connects two time-reversal invariant momentum points, the observed connectivity of the bands in the marked circle is not related to topological properties but to the fact that the Au SS lies in an inverted band gap [1].

E. Influence of the substrate band structure

Coming back to the kink structure observed in Figs. 2(a) and 2(b), the fact that it is not reproduced by our calculations in Fig. 4 indicates that the electronic band structure of the underlying W(110) substrate must play a decisive role. To verify the effect of the W substrate, Fig. 2(d) displays the overall band structure of ∼3 nm-thick Au on W(110) measured with synchrotron light at a photon energy of 62 eV along the $\overline{\Gamma} - \overline{\mathrm{K}}$ direction of the Au(111) SBZ [equivalent to the $\overline{\Gamma} - \overline{\mathrm{H}}$ direction of the W(110) SBZ, as sketched in Fig. 1(d)]. Very clearly, the dispersions of the QWS bands exhibit kinks (marked by yellow ticks) along the borders of the surface-projected band gap of W(110) [Fig. 2(c)] due to enhanced interface reflectivity of the standing electron waves

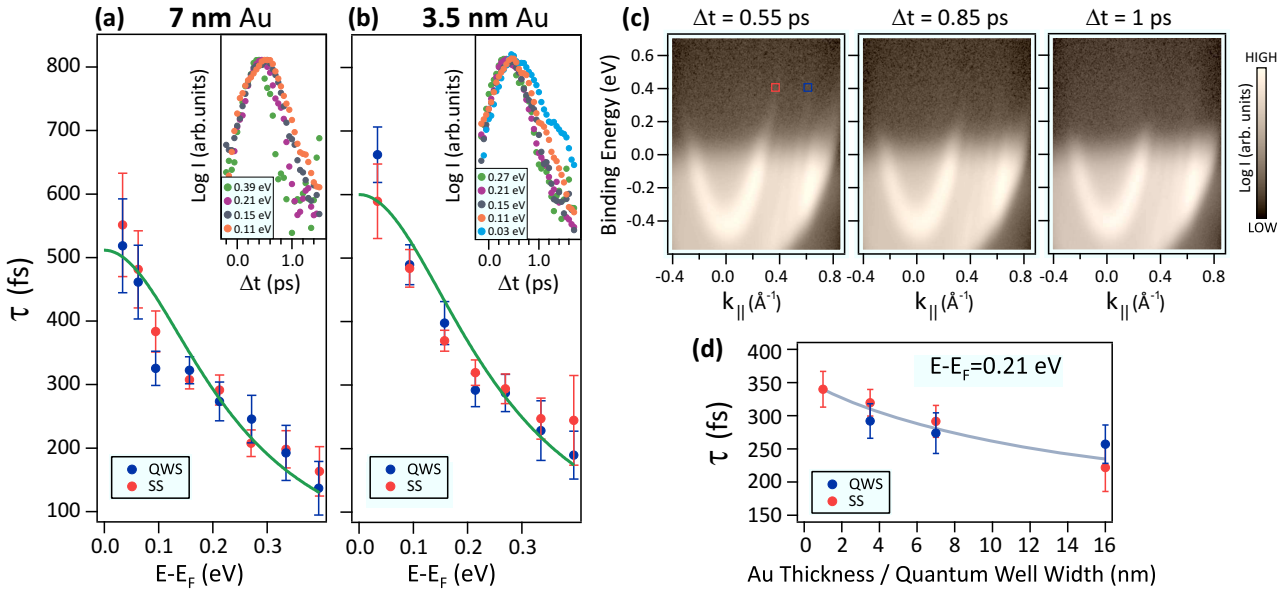

FIG. 6. (a), (b) Decay constants of surface state [red (light) color] and quantum-well states [blue (dark) color] for Au quantum films of (a) 7 nm and (b) 3.5 nm thickness. The corresponding time-resolved intensities as a function of time delay at different selected energies are shown in the insets. The data were extracted from small energy-momentum windows such as the ones shown in (c). Green (light) solid lines are fits to the data (see text). (c) From left to right, tr-ARPES dispersions at selected time delays after optical excitation. (d) Thickness dependence of the decay times at an energy of 0.21 eV above E_{F}. Gray solid line is a guide to the eye.

[14]. The linearly dispersing band of W at the border of the gap is marked by red dashed lines in Figs. 2(c) and 2(d). It crosses the Au SS dispersion just above E_{F} at nearly the same *k*-value where the kink structure appears [red arrow in figure].

We propose that the kink structure, similarly to the kinks in the QWS bands, occurs due to the influence of this linear W(110) band [which is actually an edge of the projection of the W bulk bands onto W(110)]. In Fig. 5(a), we superimpose the band structure of the 4 nm slab of Fig. 4(a) on a calculation of the bulk W substrate (gray lines). With a red circle, we highlight the approximate position of the experimentally observed kink. It is very apparent that this position coincides with the crossing of the Au SS with the linear band of W that corresponds to the red dashed line in Fig. 2(d). This theoretical result supports the experimental evidence that the presence of the substrate plays a decisive role in the appearance of the kink. To further verify the role of QWS bands, we plot in Fig. 5(b) the calculated decay of the SS wave function within several layers from the surface of the 4 nm slab. The curves are taken for the SS at four different momenta, as marked by the colored arrows in Fig. 5(a). It is clear that as we move away from the $\overline{\Gamma}$ point, the proximity to QWS bands increases and, in consequence, the SS decay length becomes longer due to the coupling to QWSs.

Therefore, we conclude that the influence of the W(110) band structure on the Au SS must be necessarily mediated by QWSs, which transfer the band structure information from the buried Au/W interface to the surface of the Au film [14]. This exclusive role of QWSs, which is inherent to the Au band structure, is further supported by the absence of a mass-renormalization kink in the SS dispersion for very thin films [left panels in Figs. 2(a) and 2(b)], meaning that in this different scenario the overall coupling picture described in Fig. 3 still holds.

F. Revealing the importance of SS-QWS coupling via electron dynamics

To further investigate if the coupling between different states is important for the appearance of the kink, we examined the ultrafast temporal evolution of the transient electron populations above E_{F} within SS and QWS bands, as shown in Fig. 6 for different widths of the quantum cavity. In particular, this type of measurements allow us to understand whether the coupling influences the relevant scattering channels responsible for charge and energy transfer between different states, and whether there is a simultaneous thermalization of carriers. In Figs. 6(a) and 6(b), we show the dependence of the decay time constants τ on the energy of excited electrons above E_{F} for two selected thicknesses of the quantum cavity (7 and 3.5 nm, respectively). The decay constants were extracted separately for the SS and QWS bands (red and blue symbols, respectively) from the exponential decay seen in the time evolution of the tr-ARPES intensities (an example for the SS at selected energies is shown in the corresponding insets). The tr-ARPES intensities were integrated at each time delay within several small energy-momentum windows distributed at different energies within the SS and QWS bands. An example of such windows is shown in Fig. 6(c), which displays snapshots of the band structure at selected time delays for a 7-nm thick film.

From the disappearance of the tr-ARPES intensity above $E_{\rm F}$, one can see that the system is almost back to equilibrium after Δt$\sim$1 ps. Moreover, excited electrons within the SS and QWS bands decay synchronously with nearly identical decay constants, behaving as dynamically-locked electron populations, which evidences the signatures of the coupling between the different states. This behavior suggests that interband scattering processes of the electrons at the surface are one of the key mechanisms underlying the simultaneous thermalization. Note that by thermalization we refer to the situation in which the whole electronic system is described by a global Fermi-Dirac distribution.

More in detail, as seen from Figs. 6(a) and 6(b), the energy dependence of τ for Au SS and QWSs follows a universal monotonic behavior that can be described as $\tau \propto (E\text{-}E_F)^{-2}$ (green solid lines). This correspondence evidences the Fermi-liquid-like behavior of charge carriers [29, 30] which is expected for hot electrons in metals [31]. However, the values of τ exceed by far the predicted decay times for the bulk system [32, 33]. The decay time τ according to Ref. [34] is given by τ^{-1}=τ_l^{-1}+$z^{-1}\tau_{FL}^{-1}$, where τ_l is an effective time constant related to the contributions of electron-phonon scattering as well as electron transport and τ_{FL} is the lifetime associated to Fermi-Liquid behavior due to inelastic electron-electron scattering. Consistent with this, from the linewidth analysis near $E_{\rm F}$ we derive an energy independent lifetime of $\sim$(11$\pm$4) fs associated with elastic impurity scattering which contributes negligibly to the measured decay times. The scaling coefficient z was introduced for Au(111) films by Cao et al. [34] and determined as 6.5 in order to eliminate the discrepancy with jellium-model-calculations by Quinn [30], providing in this way an estimation for τ_{FL} but not accounting for screening effects caused by Au $5d$ electrons. In our present work, the best fit to the experimental data of Figs. 6(a) and 6(b) provides for the 7 nm (3.5 nm) film τ_l= 511(600)$\pm$44(48) fs and z=27(38)$\pm$5(7), which supports the description of Au quantum films on W(110) in the framework of the jellium model [30]. The fact that screening effects by Au *d*-electrons are not taken into account make the model nevertheless applicable to our system since the *d*-bands in quantum wells are suppressed due to electron confinement [23, 35, 36].

G. Transversal electron transport as a benchmark for the influence of the substrate band structure

Figure 6(d) displays the thickness dependence of the decay times extracted near the region of the kink structure at an energy of 0.21 eV above $E_{\rm F}$. One can see that the decay times of SS and QWS bands increase with decreasing thickness. This behavior can also be noticed in the energy dependence of the decay times when comparing Figs. 6(a) and 6(b). There are several effects that can explain this observation. One of them is the influence of ultrafast carrier transport (ballistic or diffusive) [37–40] from the surface to the bulk of the Au film with increasing thickness. However, the efficiency of these channels should be weak, as no Au bulk states are observed in our photoemission spectra. In addition, as the SS is located within

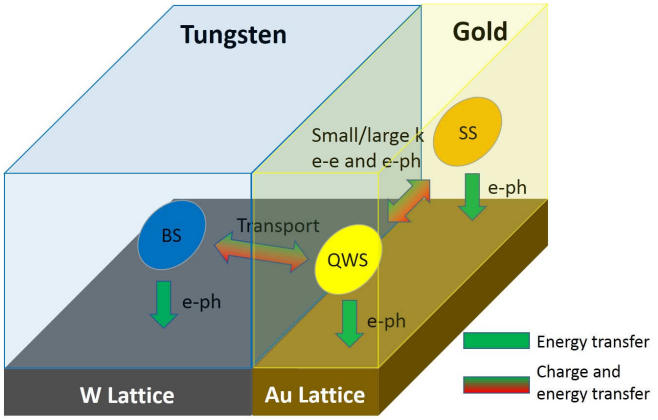

FIG. 7. Schematic representation of the main thermalization mechanisms observed in Au(111) quantum films grown on W(110). Three fundamentally different thermalization routes are highlighted: 1) electron-electron (e-e) scatterings, responsible for energy and charge transfer between surface state (SS) and quantum-well state (QWS) bands; 2) electron-phonon (e-ph) scatterings, responsible for charge transfer between bands as well as energy dissipation into the lattice; and 3) transport from surface of the film towards the substrate, leading to both charge and energy transfer between QWS bands and a continuum of W bulk states (BS). Notice how this transversal transport channel is blocked for the SS within the region of the surface-projected band gap of Au(111) (see text).

the surface-projected band gap of Au(111), there cannot be an electron transport channel from the SS to the bulk of the Au film without interband scattering because no Au bulk states are available inside the gap.

Alternatively, one might consider the opening up of electron transport channels from the surface of the Au film to the interface with the W substrate. It is known that these type of transversal transport can act as a net loss of electron population through the leakage of electrons towards the substrate. The efficiency of this process, however, ultimately depends on the electronic band-structure mismatch between overlayer and substrate. Therefore, in the most general case, this type of transport channels will be completely blocked in the region of energy-momentum space where there is a relative band gap of the substrate. For the Au SS within the region of the surface-projected gap, one can see by comparing Figs. 2(c) and 2(d) that near $E_{\rm F}$ there is a continuum of W bulk states available around $\overline{\Gamma}$. However, as the SS is strongly localized at the Au(111) surface, efficient electron transport directly from the Au SS towards the W substrate should result in faster decay times with decreasing thickness, in contrast to our observations in Fig. 6.

We do note that the continuum of W bulk states is also available for electron transport through QWSs, which due to crystal momentum conservation and the symmetry match of the propagating electrons [17, 18] continue dispersing outside and near the edge of the W gap. Thus, it is clear that transversal electron transport from the surface of the Au film towards the W substrate is necessarily mediated by QWSs, and that this

proccess cannot proceed without interband scattering which is the main mechanism responsible for the simultaneous thermalization of SS and QWS bands. The fact that both aspects are critically important in the electron dynamics is in line with our conclusion that QWSs and their coupling to the SS are key ingredients for the influence of the W substrate in the appearance of the kink.

We can finally exclude any significant role of ultrafast longitudinal transport along the direction parallel to the surface in the dynamics. Considering the large ($\sim$300 μm) lateral spot size of the pump pulse and the estimated group velocity of SS electrons ($<$0.7 nm/fs), the lateral propagation range of excited electrons will not exceed 1.5 μm (even without taking into account the electron mean-free-path which is $\sim$200-300 Å at a given kinetic energy of 2-3 eV).

H. Influence of quantum confinement on the thermalization time scales as a verification of the coupling scenario

In Fig. 7, we show a schematic representation which on the basis of our present findings summarizes the most important channels of ultrafast charge and energy transfer between different bands, as well as their energy dissipation into the lattice. Interband transitions via electron-electron and electron-phonon scatterings are predominantly responsible for the overall transfer of charge and energy between SS and QWS bands. When the separation between SS and QWS bands in energy-momentum space increases and their coupling becomes weak (see Fig. 3), the energy and charge transfer channels between SS and QWS bands become less effective because electron-electron and electron-phonon scatterings require larger k transfers, with predominance of electron-electron scatterings the higher the energy. Notice that, due to the presence of a surface band gap, intraband scattering would lead instead to different chemical potentials in the SS and QWS bands which is clearly not the case here.

In addition, quantization of electronic states with decreasing Au thickness in the direction perpendicular to the surface reduces the phase space for electron-electron scattering, causing the decay times to increase with decreasing thickness, as seen in Fig. 6(d). Quantization effects also reduce the effectiveness of electron transport towards the substrate, which together with electron-phonon scatterings being responsible for the transfer of energy into the lattice, are the only two mechanisms relevant to the dynamics in the vicinity of $E_{\rm F}$. The influence of these effects in the electron dynamics is consistent with the overall coupling scenario behind the origin of the kink structure discussed in previous sections.

It should be emphasized that, for the pump intensities employed here ($\sim 6.3\times10^8$W/cm^2), no heating of the lattice itself needs to be considered [34]. In other words, the electron-phonon coupling strength, which has been shown to be rather independent of film thickness [41], is not affected by the pump excitation itself. Taking into account that the electron-phonon scattering time in Au is about 30 fs and that $\hbar\omega_D$=15 meV where ω_D is the Debye frequency [29], we estimate that it will take about 420 fs for an electron to lose 0.21 eV. This time scale is clearly above the decay times seen in Fig. 6(d) and it cannot entirely explain the larger values of the effective time constant τ_l extracted from Figs. 6(a) and 6(b). On the one hand, this result highlights the impact of quantization effects on the efficiency of transversal electron transport near $E_{\rm F}$, which is the main reason for the increasing values of τ_l with decreasing thickness. On the other hand, it also provides further evidence for the importance of electron-electron scattering which is in any case a slow channel of thermalization due to Auger-like secondary electron emission upon recombination of the hot electron with a hole [40].

IV. SUMMARY

In conclusion, the present results offer an alternative route to engineer the band dispersion of surface states in two-dimensional metallic systems where quantum-size effects are important. Using photoemission in combination with time, energy and momentum resolution, we have accessed the band dispersion of the Shockley-type SS of two-dimensional Au(111) quantum films grown on W(110) above and below $E_{\rm F}$. Our results show that the SS dispersion significantly deviates from the parabolic behavior expected for a free-electron-like system. The deviation appears more pronounced above $E_{\rm F}$ where we observe a kink structure that is consistent with a remarkable enhancement of the SS effective mass. In combination with DFT calculations, we have analyzed various aspects that are relevant for the modification of the SS dispersion, namely the impact of strain, the influence of the substrate band structure, and the crucial role of QWSs and their coupling to the SS for the appearance of the kink. Finally, we have provided further evidence for the decisive role of the substrate band structure and the overall coupling scenario behind the origin of the kink structure through direct measurements of the electron dynamics. These measurements also reveal a unique relationship between the decay time scales and the influence of quantum confinement on the efficiency of the relevant channels responsible for ultrafast charge and energy transfer following optical excitation.

ACKNOWLEDGEMENTS

Financial support from the Impuls-und Vernetzungsfonds der Helmholtz-Gemeinschaft under grant No. HRSF-0067 (Helmholtz-Russia Joint Research Group) is gratefully acknowledged. M. B. gratefully acknowledges financial support from the Nanyang Technological University, NAP-SUG.

* Corresponding author. E-mail address: jaime.sanchez-barriga@helmholtz-berlin.de

[1] W. Shockley, Phys. Rev. **56**, 317 (1939).
[2] S. LaShell, B. A. McDougall, and E. Jensen, Phys. Rev. Lett. **77**, 3419 (1996).
[3] F. Reinert, G. Nicolay, S. Schmidt, D. Ehm, and S. Hüfner, Phys. Rev. B **63**, 115415 (2001).

[4] M. Hoesch, M. Muntwiler, V. N. Petrov, M. Hengsberger, L. Patthey, M. Shi, M. Falub, T. Greber, and J. Osterwalder, Phys. Rev. B **69**, 241401(R) (2004).

[5] E. I. Rashba, Fiz. Tverd. Tela (Leningrad) **2**, 1224 (1960); Sov. Phys. Solid State **2**, 1109 (1960).

[6] Y. A. Bychkov and E. I. Rashba, J. Phys. C: Solid State Phys. **17**, 6039 (1984).

[7] G. Bihlmayer, Y. M. Koroteev, P. M. Echenique, E. V. Chulkov, and S. Blügel, Surf. Sci. **600**, 3888 (2006).

[8] M. Nagano, A. Kodama, T. Shishidou, and T. Oguchi, J. Phys.: Condens. Matter **21**, 064239 (2009).

[9] B. Yan, B. Stadtmüller, N. Haag, S. Jakobs, J. Seidel, D. Jungkenn, S. Mathias, M. Cinchetti, M. Aeschlimann, and C. Felser, Nat. Commun. **6**, 10167 (2015).

[10] S. N. P. Wissing, C. Eibl, A. Zumbülte, A. B. Schmidt, J. Braun, J. Minár, H. Ebert, and M. Donath, New J. Phys. **15**, 105001 (2013).

[11] A. Varykhalov, D. Marchenko, J. Sánchez-Barriga, E. Golias, O. Rader, and G. Bihlmayer, Phys. Rev. B **95**, 245421 (2017).

[12] A. Varykhalov, D. Marchenko, M. R. Scholz, E. D. L. Rienks, T. K. Kim, G. Bihlmayer, J. Sánchez-Barriga, and O. Rader, Phys. Rev. Lett. **108**, 066804 (2012).

[13] J. Sánchez-Barriga, G. Bihlmayer, D. Wortmann, D. Marchenko, O. Rader, and A. Varykhalov, New J. Phys. **15**, 115009 (2013).

[14] A. Varykhalov, J. Sánchez-Barriga, A. M. Shikin, W. Gudat, W. Eberhardt, and O. Rader, Phys. Rev. Lett. **101**, 256601 (2008).

[15] `www.flapw.de`.

[16] A. Varykhalov, O. Rader, and W. Gudat, Phys. Rev. B **72**, 115440 (2005).

[17] J. J. Paggel, T. Miller, and T.-C. Chiang, Science **283**, 1709 (1999).

[18] R. K. Kawakami, E. Rotenberg, H. J. Choi, E. J. Escorcia-Aparicio, M. O. Bowen, J. H. Wolfe, E. Arenholz, Z. D. Zhang, N. V. Smith, and Z. Q. Qiu, Nature **398**, 132 (1999).

[19] T. Miller, A. Samsavar, G. E. Franklin, and T. C. Chiang, Phys. Rev. Lett. **61**, 1404 (1988).

[20] P. Moras, G. Bihlmayer, P. M. Sheverdyaeva, S. K. Mahatha, M. Papagno, J. Sánchez-Barriga, O. Rader, L. Novinec, S. Gardonio, and C. Carbone, Phys. Rev. B **91**, 195410 (2015).

[21] A. Varykhalov, A. M. Shikin, W. Gudat, P. Moras, C. Grazioli, C. Carbone, and O. Rader, Phys. Rev. Lett. **95**, 247601 (2005).

[22] J. H. Dil, F. Meier, J. Lobo-Checa, L. Patthey, G. Bihlmayer, and J. Osterwalder, Phys. Rev. Lett. **101**, 266802 (2008).

[23] P. M. Sheverdyaeva, R. Requist, P. Moras, S. K. Mahatha, M. Papagno, L. Ferrari, E. Tosatti, and C. Carbone, Phys. Rev. B **93**, 035113 (2016).

[24] E. E. Krasovskii, Phys. Rev. B **90**, 115434 (2014).

[25] H. Ishida, Phys. Rev. B **90**, 235422 (2014).

[26] T. Giela, K. Freindl, N. Spiridis, and J. Korecki, Appl. Surf. Sci. **312**, 91 (2014).

[27] A. A. Ünal, C. Tusche, S. Ouazi, S. Wedekind, C.-T. Chiang, A. Winkelmann, D. Sander, J. Henk, and J. Kirschner, Phys. Rev. B **84**, 073107 (2011).

[28] G. Neuhold and K. Horn, Phys. Rev. Lett. **78**, 1327 (1997).

[29] N. W. Ashcroft and N. D. Mermin, *Solid Sate Physics* (Holt, Rinehart and Winston, New York, 1976).

[30] J. J. Quinn, Phys. Rev. **126**, 1453 (1962).

[31] E. Knoesel, A. Hotzel, T. Hertel, M. Wolf, and G. Ertl, Surf. Sci. **368**, 76 (1996).

[32] V. M. Silkin, P. Lazić, N. Došlić, H. Petek, and B. Gumhalter, Phys. Rev. B **92**, 155405 (2015).

[33] X. Cui, C. Wang, A. Argondizzo, S. Garrett-Roe, B. Gumhalter, and H. Petek, Nat. Phys. **10**, 505 (2014).

[34] J. Cao, Y. Gao, H. E. Elsayed-Ali, R. J. D. Miller, and D. A. Mantell, Phys. Rev. B **58**, 10948 (1998).

[35] A. M. Shikin, O. Rader, G. V. Prudnikova, V. K. Adamchuk, and W. Gudat, Phys. Rev. B **65**, 075403 (2002).

[36] D.-A. Luh, J. J. Paggel, T. Miller, and T.-C. Chiang, Phys. Rev. Lett. **84**, 3410 (2000).

[37] M. Battiato, K. Carva, and P. M. Oppeneer, Phys. Rev. Lett. **105**, 027203 (2010); Phys. Rev. B **86**, 024404 (2012).

[38] M. Battiato, P. Maldonado, and P. M. Oppeneer, J. Appl. Phys. **115**, 172611 (2014).

[39] J. Sánchez-Barriga, M. Battiato, E. Golias, A. Varykhalov, L. V. Yashina, O. Kornilov, and O. Rader, Appl. Phys. Lett. **110**, 141605 (2017).

[40] F. Freyse, M. Battiato, L. V. Yashina, and J. Sánchez-Barriga, Phys. Rev. B **98**, 115132 (2018).

[41] J. Hohlfeld, S.-S. Wellershoff, J. Güdde, U. Conrad, V. Jähnke, and E. Matthias, Chem. Phys. **251**, 237 (2000).